

Study on the removal of elemental mercury from simulated flue gas by Fe₂O₃-CeO₂/AC at low temperature

Yan Wang^{1,2} · Caiting Li^{1,2} · Lingkui Zhao^{1,2} · Yin'e Xie^{1,2} · Xunan Zhang^{1,2} · Guangming Zeng^{1,2} · Huiyu Wu^{1,2} · Jie Zhang^{1,2}

Received: 27 April 2015 / Accepted: 29 October 2015 / Published online: 9 November 2015
© Springer-Verlag Berlin Heidelberg 2015

Abstract Fe₂O₃ and CeO₂ modified activated coke (AC) synthesized by the equivalent-volume impregnation were employed to remove elemental mercury (Hg⁰) from simulated flue gas at a low temperature. Effects of the mass ratio of Fe₂O₃ and CeO₂, reaction temperature, and individual flue gas components including O₂, NO, SO₂, and H₂O (g) on Hg⁰ removal efficiency of impregnated AC were investigated. The samples were characterized by Brunauer–Emmett–Teller (BET), X-ray diffraction (XRD), scanning electron microscopy (SEM), and X-ray photoelectron spectroscopy (XPS). Results showed that with optimal mass percentage of 3 % Fe₂O₃ and 3 % CeO₂ on Fe₃Ce₃/AC, the Hg⁰ removal efficiency could reach an average of 88.29 % at 110 °C. Besides, it was observed that O₂ and NO exhibited a promotional effect on Hg⁰ removal, H₂O (g) exerted a suppressive effect, and SO₂ showed an insignificant inhibition without O₂ to some extent. The analysis of XPS indicated that the main species of mercury on used Fe₃Ce₃/AC was HgO, which implied that adsorption and catalytic oxidation were both included in Hg⁰ removal. Furthermore, the lattice oxygen, chemisorbed oxygen, and/or weakly bonded oxygen species made a contribution to Hg⁰ oxidation.

Keywords Elemental mercury · Activated coke · Adsorption · Catalytic oxidation · Flue gas · Low temperature

Introduction

Mercury is a global pollutant because of its toxicity, mobility, and bioaccumulation in the ecosystem and food chain (Pavlish et al. 2003). The emission of mercury from anthropogenic sources is a serious concern that attracts considerable public attention. Coal-fired power plants are considered to be a major source of anthropogenic mercury emissions. By April 2010, more than 20 states in the USA had issued mercury emission regulations to regulate mercury emissions from coal-fired power plants which were more stringent than the Clean Air Mercury Rule (CAMR) (Milford and Pieniak 2009). In order to control mercury emission from coal-fired power plants, the Mercury and Air Toxics Standards (MATS) announced in 2011 by the US Environment Protection Agency (USEPA) emphasized the control of mercury, acid gases, and other toxic pollutants (Zhang et al. 2014). Therefore, it is an extremely urgency to find effective technologies to control mercury emission.

Mercury in coal-fired flue gas is generally presented in three forms, namely elemental mercury (Hg⁰), oxidized mercury (Hg²⁺), and particle-bound mercury (Hg^p) (Galbreath and Zygarlicke 2000). Hg^p and Hg²⁺ are relatively easy to be removed by typical air pollution control devices (APCDs). For instance, Hg^p can be captured by particulate matter (PM) control devices such as electrostatic precipitators (ESPs) and fabric filters (FFs). Hg²⁺ is soluble in water, and it can be removed efficiently by wet flue gas desulfurization equipments (WFGDs) (Hsi et al. 2010). However, Hg⁰ can hardly be removed by currently available APCDs for its high volatility and nearly insolubility in water, which becomes the biggest obstacle for mercury control.

Responsible editor: Philippe Garrigues

✉ Caiting Li
ctli@hnu.edu.cn; cti3@yahoo.com

¹ College of Environmental Science and Engineering, Hunan University, Changsha 410082, People's Republic of China

² Key Laboratory of Environmental Biology and Pollution Control, Hunan University, Ministry of Education, Changsha 410082, People's Republic of China

Up to now, sorbents/catalysts like carbon-based sorbents, selective catalytic reduction (SCR) catalysts, and metals or metal oxides (Cao et al. 2007; Presto and Granite 2006) have been used for Hg^0 removal. Among them, Hg^0 removal with activated carbon has been proved to be an effective technique in commercial application by many researchers (Li et al. 2003). However, the activated carbon owns a distinct disadvantage of high cost. Activated coke (AC) is a kind of porous activated carbon-based sorbent which is not adequately activated. With high mechanical strength, AC could endure attrition and comminution during circulation and handling processes (Jastrzab 2012). AC in granular form is suited to be used in both moving bed and fixed-bed unit. Meanwhile, AC inherits the virtues of activated carbon such as the structure characteristics, adsorption and catalytic properties, physical and chemical stability (Li et al. 2013). In addition, AC can suffice for handling lots of pollutants such as H_2S , SO_2 , NH_3 , and Hg in exhaust gas under the corresponding temperature (Itaya et al. 2009; Ogriseck and Vanegas 2010; Shawwa et al. 2001).

Due to high volatility and weak bonding onto carbon surface of Hg^0 , suitable chemical modifications on AC are sought to boost its adsorption and catalytic performance for Hg^0 removal. Recently, various transition-metal oxides including Fe_2O_3 , V_2O_5 , CuO , CeO_2 , MnO_2 , Mn_2O_3 , Cr_2O_3 , and RuO_2 had been widely investigated as potential Hg^0 oxidation catalysts, and these metal oxides were valid for oxidizing Hg^0 to Hg^{2+} (Dunham et al. 2003; Fan et al. 2012; Ji et al. 2008; Kamata et al. 2009; Pitoniak et al. 2005; Yan et al. 2011). Thereinto, CeO_2 plays an important role in a large number of catalytic reactions, and it has been extensively studied as an oxygen provider by storing or releasing O_2 via the unique $\text{Ce}^{4+}/\text{Ce}^{3+}$ redox couple (Kaspar et al. 1999). Owing to the redox shift between Ce^{3+} and Ce^{4+} , labile oxygen vacancies and bulk oxygen species with relatively high mobility can be easily formed (Reddy et al. 2003), which make them active for oxidation process. Thus, CeO_2 has been successfully applied to important processes such as catalytic wet oxidation and CO oxidation (Ayastuy et al. 2006; Delgado et al. 2006). Additionally, Kinya et al. reported that the impregnation of Fe on the active carbon greatly enhanced the removal of both COS and H_2S at 300–450 °C (Sakanishi et al. 2005). In Fe-Mn mixed oxides, iron cations are replaced by manganese cations and an equivalent number of cation vacancies are incorporated to maintain the spinel structure (Gillot et al. 1997). Yue et al. (Yue and Zhang 2009) reported that incorporation of Fe^{3+} into fluorite structure of CeO_2 induces oxygen-storage systems and can give rise to the increase of oxide ion vacancies which are responsible for their high solid-state ionic conductivity. Consequently, CeO_2 coupled with Fe_2O_3 modified AC may have high removal efficiency for Hg^0 . To our knowledge, there is little information about Fe_2O_3 and CeO_2 modified AC for Hg^0 removal.

In this study, AC is used as a supporter to synthesize Fe_2O_3 - CeO_2 /AC samples by the equivalent-volume

impregnation method. Different operation parameters like reaction temperature and individual flue gas components on Hg^0 removal were studied and optimized. Various characterization methods were applied to study the structure and physicochemical characteristic of samples. The ultimate goal of this study is to develop an economical sorbent which is promising for industrial application in Hg^0 removal from coal-fired flue gas.

Experimental section

Samples preparation

The AC (columnar granules with a length of 7–9 mm and an average diameter of 5 mm) used in the experiment was obtained from Inner Mongolia Kexing Carbon Industry Limited Liability Company. The samples were prepared by the equivalent-volume impregnation method as follows: At first, AC was washed with deionized water for several times and dried in an electric blast oven at 105 °C for 12 h. After that, different amount of $\text{Ce}(\text{NO}_3)_3 \cdot 6\text{H}_2\text{O}$ and $\text{Fe}(\text{NO}_3)_3 \cdot 9\text{H}_2\text{O}$ were dissolved in deionized water to form mixed solution. Then, a certain amount of AC was impregnated in the solution for 18 h. After impregnation, the samples were dried in an electric blast oven at 105 °C for 12 h and calcinated in an electric tube furnace at 450 °C for 4 h under N_2 atmosphere. Finally, the samples were cooled down to room temperature and stored in a desiccator for further use. Fe_2O_3 - CeO_2 /AC samples were denoted as FexCey/AC , where Fe represents Fe_2O_3 , Ce represents CeO_2 , x and y represent the mass percentage of Fe_2O_3 and CeO_2 on the total sample mass including AC, Fe_2O_3 , and CeO_2 , respectively. In the entire experimental procedure, the total mass percentage of Fe_2O_3 and CeO_2 on all samples was 6 %, which was based on our previous work (Xie et al. 2015). Meanwhile, Fe/AC and Ce/AC were prepared with the same method mentioned above.

Samples characterization

Brunauer–Emmett–Teller (BET) was performed by using a TriStarII3020 analyzer (Mcpicromeritics Instrument Corp, USA) to determine the specific surface area and porosity of samples. All of the samples were degassed at 180 °C for 5 h prior to BET measurements.

X-ray diffraction (XRD) measurements were carried out on a Bruker D8-Advance device to examine the crystallinity and dispersivity of iron and cerium species on AC surface using $\text{CuK}\alpha$ radiation ($\lambda=0.1543$ nm) in the range of 10–80° (2 θ) with a step size of 0.02°.

To further analyze the morphology and surface structure of the samples, scanning electron microscopy (SEM) photographs were obtained by means of a HITACHI S-4800 analyzer.

X-ray photoelectron spectroscopy (XPS) analysis was carried out on a K-Alpha 1063 X-ray photoelectron spectrometer (Thermo Fisher Scientific, USA) with an Al Ka X-ray source at room temperature. The binding energies were calibrated by the C 1 s peak at 284.6 eV.

Experimental setup and procedure

Figure 1 shows the schematic diagram of the experimental system, which consisted of a simulated flue gas system, Hg⁰ vapor-generating device, electric tube furnace reactor, and an online mercury analyzer. The simulated flue gas (SFG) contained 70 μg/m³ Hg⁰, 5 % O₂, 8 % H₂O (when used), 300 ppm NO, 400 ppm SO₂, 12 % CO₂, and balanced N₂. A flow of high-purity nitrogen (200 ml/min) was used as Hg⁰-laden gas stream by passing through the Hg⁰ permeation tube (VICI Metronics). To guarantee a constant permeation concentration, the Hg⁰ permeation tube was placed in a U-shaped quartz tube, which was immersed in an electric-heated thermostatic water bath. The total flow rate was controlled at 1 L/min in each test using mass flow controllers, corresponding to a space velocity of about 4200 h⁻¹. The electric tube furnace was comprised of a quartz tube (a length of 95 cm and an inner diameter of 52 mm) and matched installations for regulating the reaction temperature. The inlet and outlet Hg⁰ concentrations were measured by the mercury

analyzer (Lumex RA-915 M, Russia). The exhaust gas from the mercury analyzer was introduced into an activated carbon trap before released into the atmosphere.

Five sets of experiments were carried out and the reaction conditions are listed in Table 1. Set 1 experiments were aimed at determining the optimal mass ratio of Fe₂O₃ and CeO₂. The Hg⁰ removal activity over virgin AC and impregnated AC was evaluated under SFG for 3 h. In Set 2, the optimal sample was tested in SFG at each selected reaction temperature for investigating the optimal reaction temperature. The roles of individual flue gas components on Hg⁰ removal and the reaction pathways were explored in Set 3 experiments, which were conducted on the optimal sample in the presence of individual flue gas (balanced with N₂ or O₂ plus N₂) at optimal operating temperature. In Set 4 experiments, the optimal sample was tested in SFG for 14 h at optimal operating temperature for studying its durability. Set 5 experiments investigated the breakthrough curves of Hg⁰ captured by the optimal sample under N₂ and N₂ plus O₂.

During each experiment, the flue gas firstly bypassed the fix-bed reactor until a stable inlet concentration of Hg⁰ was obtained. When the mercury analyzer had been stable for more than 30 min, the gas flow was switched to pass through the sample and Hg⁰ concentration in the outlet was measured. At last, the gas flow bypassed the reactor again so as to verify the inlet concentration of Hg⁰. Meanwhile, a mercury conversion system coupled with RA-915 M mercury analyzer was

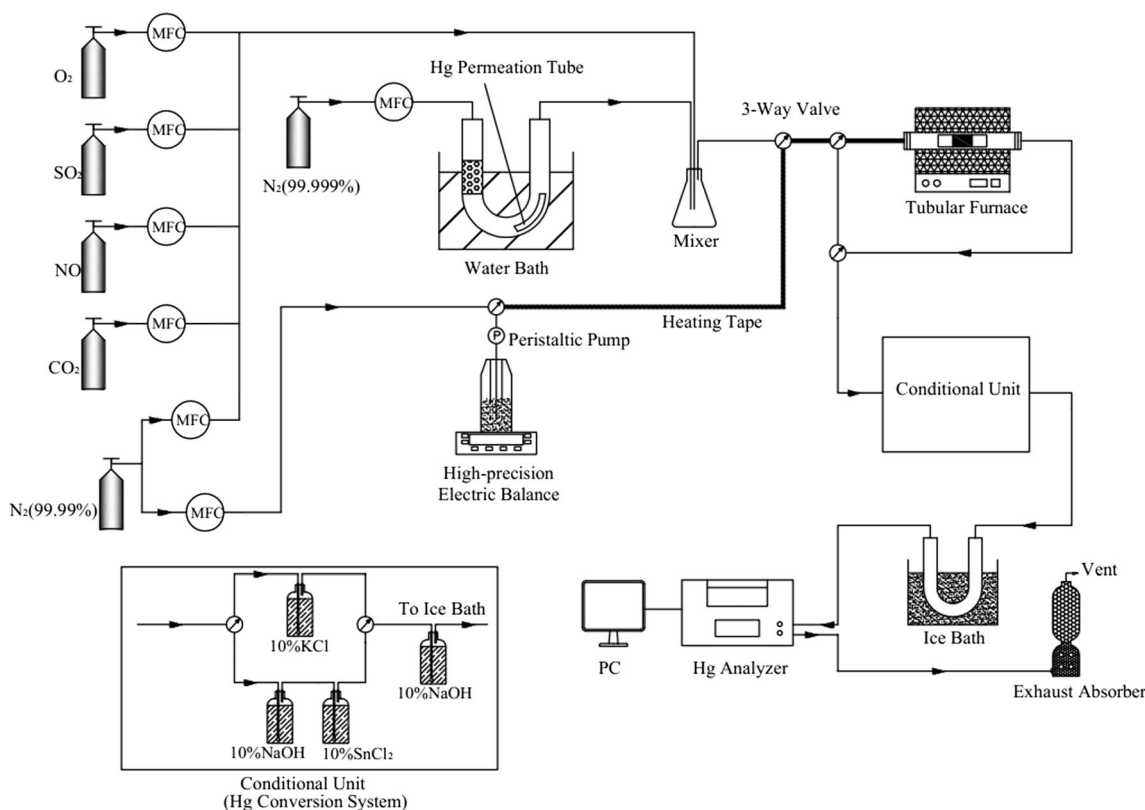


Fig. 1 Schematic diagram of the experimental setup

Table 1 The experimental reaction conditions

Experiment	Sample	Flue gas components	Temperature (°C)
Set 1	AC, Ce6/AC, Fe1Ce5/AC, Fe2Ce4/AC, Fe3Ce3/AC, Fe4Ce2/AC	SFG(N ₂ , 5 % O ₂ , 12 % CO ₂ , 300 ppm NO, 400 ppm SO ₂)	110
Set 2	The optimal sample	SFG(N ₂ , 5 % O ₂ , 12 % CO ₂ , 300 ppm NO, 400 ppm SO ₂)	50~200
Set 3	The optimal sample	N ₂ /(N ₂ +O ₂)+individual flue gas components (NO, SO ₂); SFG/SFG+8 % H ₂ O	The optimal temperature
Set 4	The optimal sample	SFG(N ₂ , 5 % O ₂ , 12 % CO ₂ , 300 ppm NO, 400 ppm SO ₂)	The optimal temperature
Set 5	The optimal sample	N ₂ /(N ₂ +5 % O ₂)	The optimal temperature

employed to measure Hg⁰ and Hg²⁺ concentrations in outlet flue gas. As shown in Fig. 1, in the mercury conversion system, gas stream released from the reactor was divided into two streams, one for measuring total mercury (Hg^T) and the other for elemental mercury (Hg⁰). On one stream, an impinger with 10 wt% acidic stannous chloride (SnCl₂) solution was used to measure Hg^T, since acidic SnCl₂ solution can reduce Hg²⁺ to Hg⁰ which can then be detected by the mercury analyzer. On the other stream, an impinger containing 10 wt% potassium chloride (KCl) solution was used to measure Hg⁰, because KCl solution can capture Hg²⁺ and allow only Hg⁰ to pass through. Before the sampling gas entered the SnCl₂ solution, a 10 wt% sodium hydroxide (NaOH) solution was used to remove SO₂. The concentration of Hg²⁺ in outlet flue gas could then be calculated by the difference between Hg^T and Hg⁰. At the end of the conversion system, the two streams converged to a 10 wt% NaOH solution in which acid gases were captured to avoid corrosion of the detection cell in the mercury analyzer. Supposing mercury absorbed on AC was thoroughly in oxidation state. Therefore, the Hg⁰ removal efficiency (E_{oxi}) was quantified by the following equation:

$$E_{\text{oxi}}(\%) = \frac{[\text{Hg}^0]_{\text{in}} - [\text{Hg}^0]_{\text{out}}}{[\text{Hg}^0]_{\text{in}}} \times 100\% \quad (1)$$

Where [Hg⁰]_{in} and [Hg⁰]_{out} represent Hg⁰ concentration (μg/m³) at the inlet and outlet of the reactor, respectively. Since the mercury discharged from reactor includes both Hg⁰ and Hg²⁺, the Hg⁰ capture efficiency (E_{cap}) was introduced to be calculated by the formula below:

$$E_{\text{cap}}(\%) = \frac{[\text{Hg}^0]_{\text{in}} - [\text{Hg}^{\text{T}}]_{\text{out}}}{[\text{Hg}^0]_{\text{in}}} \times 100\% \quad (2)$$

Where [Hg⁰]_{in} represents Hg⁰ concentration (μg/m³) in inlet of the reactor, and [Hg^T]_{out} represents Hg^T concentration (μg/m³) in outlet of the reactor.

Results and discussion

Samples characteristics

BET analysis

The physical properties of virgin AC and impregnated AC including BET surface area, pore volume, and average pore size are summarized in Table 2. The results showed that the modification increased BET surface area and pore volume. During impregnation and calcination, a certain number of new pores might be generated due to the reaction between AC and active components, which account for higher BET surface area of impregnated AC compared to virgin AC. However, the increasing doping of Fe₂O₃ reduced the BET surface area and pore volume of AC to some extent except for Fe4Ce2/AC. Especially, it can be observed that Fe3Ce3/AC had the lowest BET surface area of 276.74 m²/g and minimum pore volume of 0.14 cm³/g among impregnated AC. The result could be explained as follows: On one hand, it was possibly resulted from the deterioration of some of the thin pore walls on AC over strong oxidation of Fe-Ce mixed oxides. On the other hand, the internal pores might be blocked when Fe₂O₃ and CeO₂ particles enter into the interior of pores (Wen et al. 2011).

Table 2 BET surface areas and pore parameters of the samples

Sample	BET surface area (m ² /g)	Total pore volume (cm ³ /g)	Average pore size (nm)
AC	271.5727	0.1331	1.9608
Fe1Ce5/AC	329.5082	0.1565	1.9001
Fe2Ce4/AC	324.3651	0.1602	1.9752
Fe3Ce3/AC	276.7377	0.1379	1.9926
Fe4Ce2/AC	284.6674	0.1472	2.0677

XRD analysis

The XRD patterns of virgin AC, Ce6/AC, Fe2Ce4/AC, Fe3Ce3/AC, and Fe4Ce2/AC are presented in Fig. 2. Two diffraction peaks attributed to AC were detected at 26.66° and 44.58°. Nevertheless, the two peaks even disappeared when the mass ratio of Fe₂O₃ and CeO₂ was above 2:4, indicating that Fe₂O₃ and CeO₂ interacted with AC strongly in these samples. The peaks at 27.88°, 32.96°, 46.98°, and 56.14° were corresponding to CeO₂, which could be detected over Ce6/AC. When the mass ratio of Fe₂O₃ and CeO₂ was 2:4, 3:3, 4:2, there was no obvious peaks belong to CeO₂ or Fe₂O₃. It may be explained that Fe₂O₃ and CeO₂ existed as an amorphous phase or highly dispersed on the surface of AC. When the mass percentage of Fe single oxide was increased to 30 %, it could be seen that Fe mainly presented in the form of Fe₂O₃. Peaks with strong intensity appeared at 30.52°, 35.74°, 43.07°, and 62.68° which were matched well with peaks of Fe₂O₃. In addition, the peaks attributed to CeO₂ had strong intensity for Fe15Ce15/AC. This implied that the synergy of Fe₂O₃ and CeO₂ probably led to an excellent dispersion of active components on the surface of AC when the overall loading value was 6 %.

SEM analysis

Figure 3 shows SEM micrographs of virgin AC and the selected impregnated AC. The characteristics of AC surface have changed according to different active components loading. As shown in Fig. 3d, Fe₂O₃ and CeO₂ were widely dispersed on the AC surface and only a few agglomerates existed in Fe3Ce3/AC. Furthermore, there were more small holes on the surface of Fe3Ce3/AC compared with other samples, which indicated that Fe₂O₃ and CeO₂ extensively modified the structure of AC. However, in the case of Fe4Ce2/AC, the agglomerates became bigger. Consequently, there were

synergistic effects between Fe₂O₃ and CeO₂, so the interaction could improve the dispersion of Fe₂O₃ and CeO₂ on the surface of AC and then improved the Hg⁰ removal efficiency. Moreover, the phenomenon was in accordance with XRD analysis. According to the refs (Huang et al. 2009; Sahoo et al. 2009; Wan et al. 2009), cerium can enhance the catalytic property owing to the MO_x-CeO_x (M=Fe, Cu and Pd) interaction. In our study, doped samples with layer of Fe₂O₃ and CeO₂ covered on certain surface of the sorbents could provide enough oxidation capacity.

XPS analysis

To determine the chemical state and the relative portion of the main elements on the surface of different samples, fresh Fe3Ce3/AC and used Fe3Ce3/AC were investigated by XPS technique. The XPS spectra over the spectral regions of O 1 s, Fe 2p, Ce 3d, and Hg 4f are shown in Fig. 4.

In Fig. 4a, b, for fresh Fe3Ce3/AC, the O 1 s spectrum was divided into two main peaks. A binding energy of about 530.2 eV was ascribed to the lattice oxygen (denoted as O_α) in the metal oxides. The peak at higher binding energy (about 531.5 eV) belonged to chemisorbed oxygen and/or weakly bonded oxygen species (denoted as O_β), which were regarded as the most active oxygen and played an important role in oxidation reaction (Gao et al. 2010; Kang et al. 2007; Li et al. 2011a, b). For used Fe3Ce3/AC, the peak with a binding energy of about 530.3 eV was attributed to the lattice oxygen (Liu et al. 2006), while the binding energy of 532.2 eV represented chemisorbed and/or weakly bonded oxygen (as in carbonyl or carboxyl groups) (Huang et al. 2005; Liu et al. 2006). The fitted peak of O 1 s in the vicinity of 532.6 eV corresponded to oxygen in hydroxyl and/or surface adsorbed water (denoted as O_γ) (Eom et al. 2008; Gao et al. 2010).

Hypothetically, the atomic concentration of total oxygen on AC was denoted by O_T. After comparison of O 1 s profiles in fresh Fe3Ce3/AC and used Fe3Ce3/AC, the ratio of O_α/O_T clearly decreased from 33.58 to 7.43 %. In this regard, it could be inferred that lattice oxygen took part in the reaction of removing Hg⁰. Besides, the value of O_β/O_T obviously decreased from 66.42 to 40.55 % after the adsorption and oxidation reaction. This clearly manifested that some chemisorbed oxygen and/or weakly bonded oxygen species were consumed in Hg⁰ removal.

The XPS spectra of Fe 2p on fresh Fe3Ce3/AC and used Fe3Ce3/AC are shown in Fig. 4c, d. Iron ions in FeO are characterized by the Fe2p_{3/2} binding energy in the range of 709.8–710.6 eV (Descostes et al. 2000; Graat and Somers 1996), so the peaks at 710.4 and 710.6 eV referred to Fe²⁺ cations. The binding energy concentrated on 711.6 eV was typical characteristic of Fe³⁺ (Xu et al. 007). After Hg⁰ was captured, the binding energy centered at about 712.1 eV which might be ascribed to Fe³⁺ cations bonded with hydroxyl

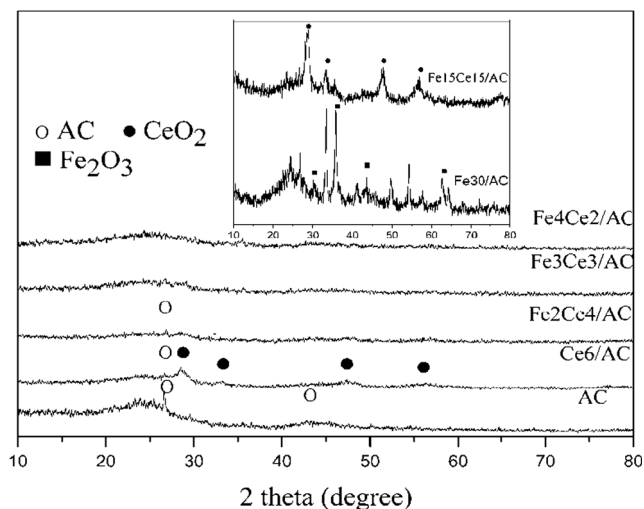
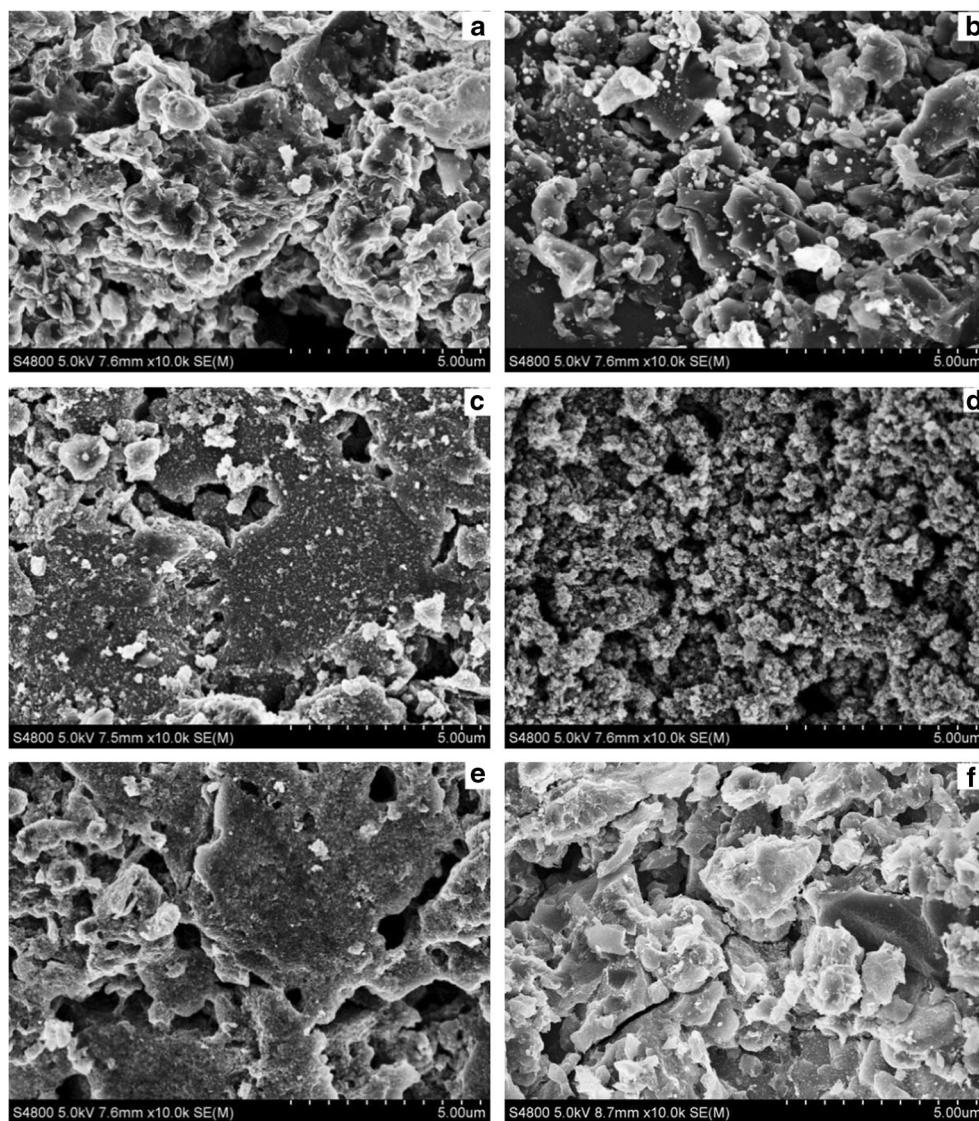


Fig. 2 XRD spectra of virgin AC and the FexCey/AC samples

Fig. 3 SEM micrographs of a virgin AC, b Ce6/AC, c Fe2Ce4/AC, d Fe3Ce3/AC, e Fe4Ce2/AC, f Fe6/AC



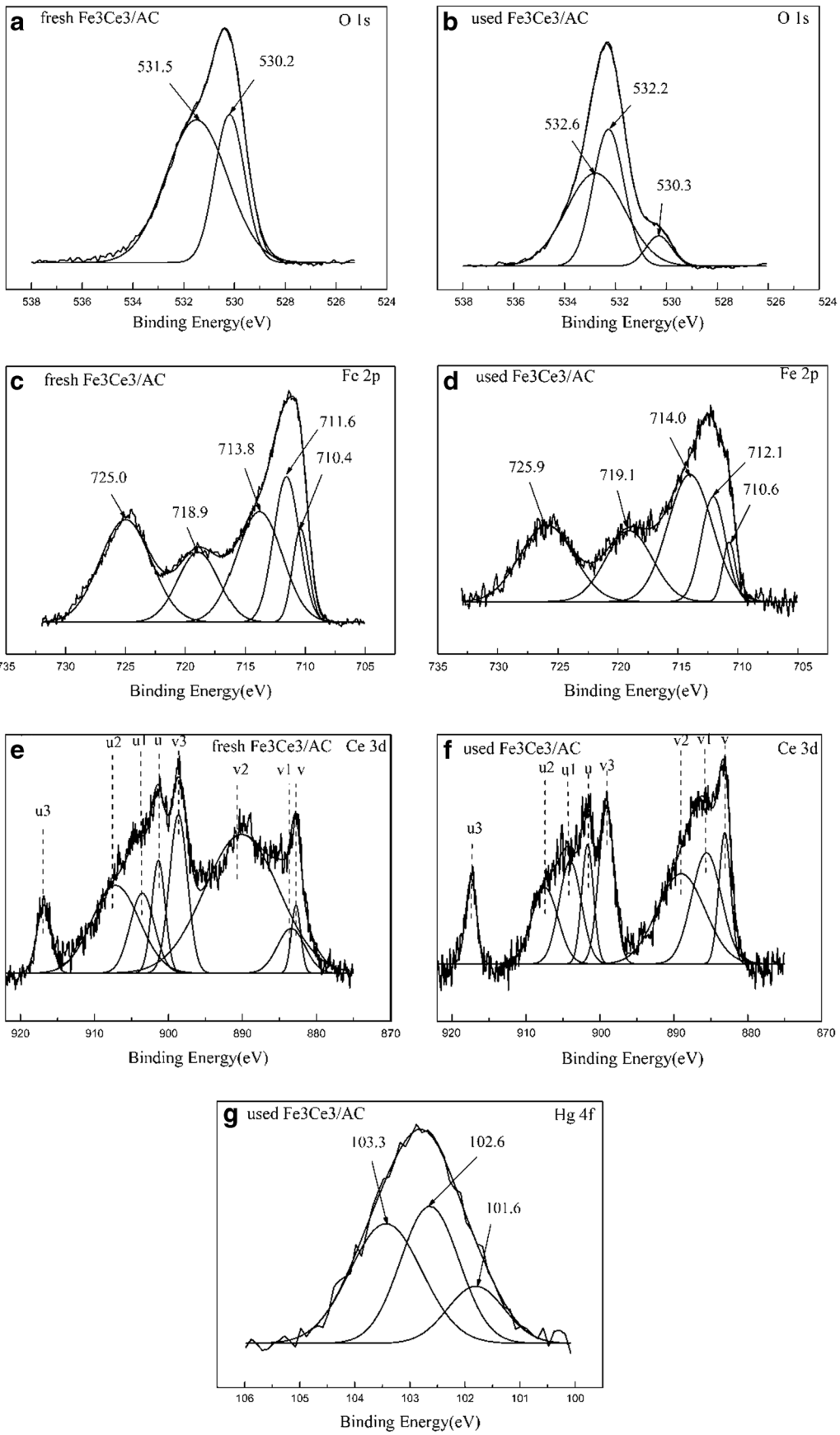
groups($\equiv\text{Fe}^{\text{III}}\text{-OH}$). Furthermore, the peak at about 719 eV was the fingerprint of Fe^{3+} species (Shen et al. 2010). After Hg^0 removal, a few changes concerning the proportion of valence happened.

Complicated XPS spectra of Ce 3d for fresh Fe3Ce3/AC and used Fe3Ce3/AC are presented in Fig. 4e, f. The peaks labeled u are due to 3d3/2 spin-orbit states, and those labeled v are the corresponding 3d5/2 states (Reddy et al. 2003). The u/v, u2/v2, and u3/v3 doublets represent the $3d^{10}4f^0$ state of Ce^{4+} , while the doublet labeled u1/v1 represents the $3d^{10}4f^1$ initial electronic state corresponding to Ce^{3+} (Mullins et al. 1998). It was apparent that Ce^{4+} and Ce^{3+} were coexisting. The presence of Ce^{3+} could create charge imbalance, vacancies, and unsaturated chemical bonds on the surface of samples (Yang et al. 2006), which lead to the increase of surface chemisorbed oxygen. Based on the peak areas, Ce^{4+} is the predominant form and considered to be advantageous for Hg^0 oxidation (Wan et al. 2011)). The ratio of $\text{Ce}^{4+}/\text{Ce}^{3+}$

decreased from 6.42 to 2.26 after removing Hg^0 , which manifested a reduction of Ce^{4+} during Hg^0 oxidation reaction.

The XPS spectrum of Hg 4f for used Fe3Ce3/AC is shown in Fig. 4g. The binding energy centered at approximate 103.3 eV was attributed to Si 2p electron (Hua et al. 2010). The peak appeared at about 101.6 eV was assigned to HgO (Ji et al. 2008). However, no adsorbed Hg^0 was found on the sample surface, which might be explained that the content of Hg^0 was lower than the detection limit of XPS analysis or the adsorbed Hg^0 desorbed from the surface of sample. Considering the results of O 1s and Hg 4f, it could be certified that HgO was the product of oxygen-containing groups and Hg^0 , both of which were absorbed weakly on the sample surface.

Fig. 4 O 1s, Fe 2p, Ce 3d, and Hg 4f XPS spectra of fresh Fe3Ce3/AC and used Fe3Ce3/AC



Performance of the samples

Screening of the optimal sample

Figure 5 presents the effect of different mass ratio of Fe_2O_3 and CeO_2 on Hg^0 removal efficiency. In comparison to virgin AC, AC modified with Fe_2O_3 and CeO_2 , particularly when the mass ratio of Fe_2O_3 and CeO_2 was 3:3, promoted the Hg^0 removal significantly. Hg^0 removal ability was enhanced with the increase of Fe_2O_3 when loading value was below 3 % and then slightly decreased with increasing Fe_2O_3 loading value to 4 %. Table 2 shows that Fe3Ce3/AC has the lowest BET surface area among impregnated AC. What's more, Fe1Ce5/AC with the largest BET surface area has the minimum Hg^0 removal efficiency of 73.89 % except for virgin AC. It indicated that Hg^0 removal was mainly influenced by the oxidation reaction and less affected by BET surface area which could affect physical adsorption. Besides, the synergy between Fe_2O_3 and CeO_2 should be a rational reason for the excellent performance of Fe3Ce3/AC. The aforementioned phenomenon was consistent with the result of SEM analysis. From the analysis above, it could be concluded that Hg^0 removal was attributed to the combination of adsorption and oxidation. Furthermore, the lattice oxygen, chemisorbed oxygen, and/or weakly bonded oxygen species made a contribution to Hg^0 oxidation. Specially, the reaction mechanism of Hg^0 removal could be explicated as follows: gaseous Hg^0 was firstly adsorbed on the sample surface to form $\text{Hg}^0(\text{ad})$, then $\text{Hg}^0(\text{ad})$ would react with the lattice oxygen which was released from Fe_2O_3 and CeO_2 to form $\text{HgO}(\text{ad})$. The possible reactions can be described as follows:

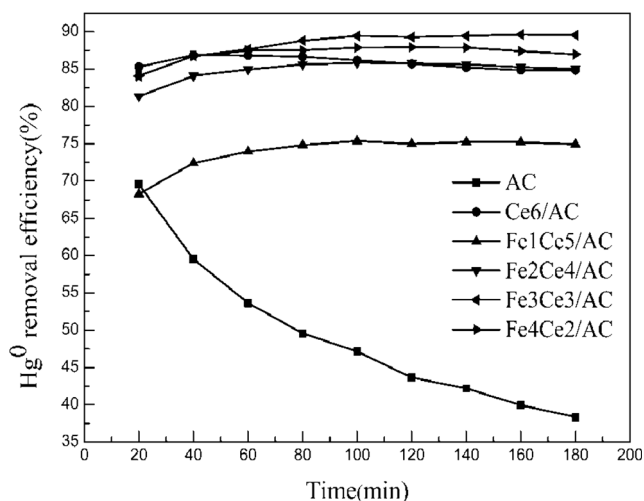
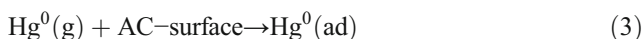


Fig. 5 Effect of the mass ratio of Fe_2O_3 and CeO_2 on Hg^0 removal efficiency. Reaction conditions: $70 \mu\text{g}/\text{m}^3 \text{Hg}^0$, 5 % O_2 , 300 ppm NO , 400 ppm SO_2 , 12 % CO_2 , N_2 as balance, $\text{GHSV}=4200 \text{ h}^{-1}$, $T=110 \text{ }^\circ\text{C}$



Furthermore, in order to explore the material balance among the amounts of Hg^0 in the inlet and the outlet streams and the one captured by the adsorbent, a related experiment was carried out. In the experiment (the reaction condition was the same as Set 4 in Table 1), a mercury conversion system coupled with RA-915 M Mercury Analyzer was used to determine the concentration of Hg^0 and Hg^{2+} in outlet flue gas. As shown in Table 3, it could be found that E_{oxi} and E_{cap} were nearly the same to each other, which indicated that the formed HgO was captured on the Fe3Ce3/AC. The result was in accordance with the analysis of XPS.

Screening of reaction temperature

A set of experiments were carried out to explore reaction temperatures (50–200 °C) on Hg^0 removal. The results given in Fig. 6 showed that Hg^0 removal efficiency increased with increasing the temperature from 50 to 110 °C and then decreased with the temperature rising from 110 to 200 °C. This phenomenon might be explained by the inhibition of physical adsorption of Hg^0 at relatively high temperature. Therefore, a range of correspondingly low temperature was beneficial for the reaction between Hg^0 and oxygen functional groups. So, the optimal temperature of 110 °C was chosen for further study.

To further investigate the durability of Hg^0 removal over Fe3Ce3/AC in SFG, the breakthrough curve of Hg^0 capture was carried out at 110 °C. As shown in Fig. 7, the C/C_0 achieved an average value of 0.13 during the 14 h reaction, which implied excellent endurance with high activity of Fe3Ce3/AC.

Effects of individual flue gas components

Effect of O_2

The Hg^0 removal efficiency over Fe3Ce3/AC at 110 °C under pure N_2 gas was observed to be around 46.00 %, as shown in Fig. 8. The loss of Hg^0 in the absence of O_2 could be ascribed to the consumption of lattice oxygen over the sample (He et al. 2014). When 5 % O_2 was introduced to gas flow, the Hg^0 removal efficiency increased to about 71.33 %. However, further increasing the O_2 concentration to 8 %, the Hg^0 removal

Table 3 The Hg^0 removal/capture efficiency of Fe3Ce3/AC

Time (h)	Inlet Hg^0 ($\mu\text{g}/\text{m}^3$)	Outlet Hg^T ($\mu\text{g}/\text{m}^3$)	Outlet Hg^0 ($\mu\text{g}/\text{m}^3$)	E_{oxi} (%)	E_{cap} (%)
1	70.36	5.52	5.06	92.81	92.15
2	70.60	4.87	4.50	93.63	93.10
3	69.98	4.81	4.43	93.67	93.13

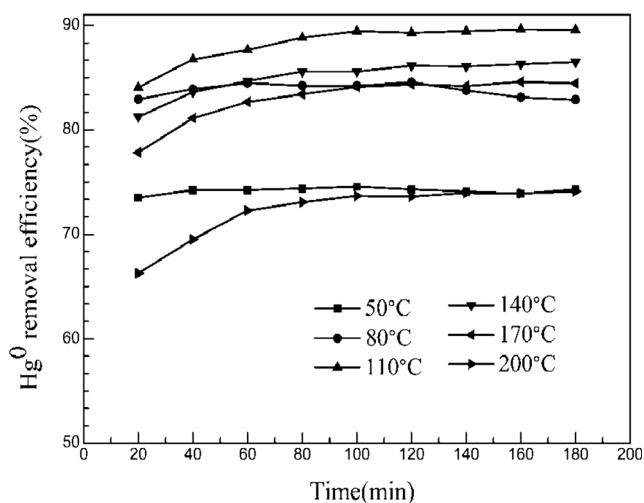


Fig. 6 Effect of reaction temperature on Hg⁰ removal efficiency. Reaction conditions: 70 μg/m³ Hg⁰, 5 % O₂, 300 ppm NO, 400 ppm SO₂, 12 % CO₂, N₂ as balance, GHSV=4200 h⁻¹, T=50, 80, 110, 140, 170, 200 °C

efficiency did not increase any more. This result suggested that 5 % O₂ would achieve the supplement for consumed lattice oxygen and was sufficient to sustain Hg⁰ oxidation.

As illustrated in Fig. 9, the Fe3Ce3/AC has a relatively high activity in the presence of O₂. When Hg⁰ vapor was introduced into (N₂/5 % O₂) mixture, O₂ was found to have the capability of promoting Hg⁰ oxidation. Unlike the test with N₂, the Hg⁰ removal efficiency was consistently much higher in (N₂/5 % O₂) mixture for the whole 12 h. Many researchers have put forward that active oxygen can be generated from adsorbed oxygen via cerium species (Deng et al. 2011; Wang et al. 2013). So O₂ would provide metal oxides with oxygen to make sure that Hg⁰ oxidation could be sustained. Combined with the results of XPS, it indicated that

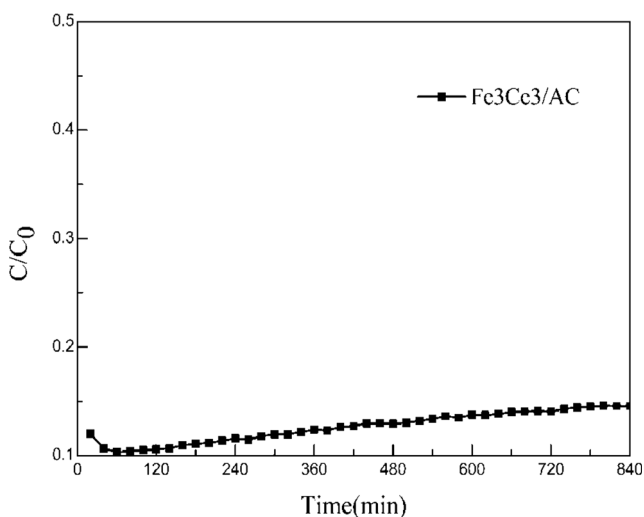


Fig. 7 The breakthrough curve of elemental mercury captured by Fe3Ce3/AC under simulated flue gas. Reaction conditions: 70 μg/m³ Hg⁰, 5 % O₂, 300 ppm NO, 400 ppm SO₂, 12 % CO₂, N₂ as balance, GHSV=4200 h⁻¹, T=110 °C

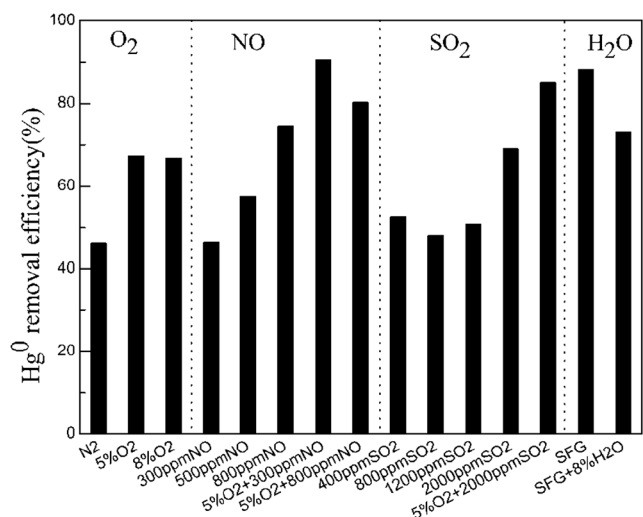


Fig. 8 Effect of individual flue gas components on Hg⁰ removal efficiency. Reaction conditions: GHSV=4200 h⁻¹, T=110 °C

the re-oxidization of formed Ce³⁺ and Fe²⁺ cations (reactions (7)–(8)) happened. Under the sufficient gas-phase O₂ supply, some cation vacancies may be recovered. Reactions involved can be expressed as follows:



Effect of NO

Compared with pure N₂ gas, an addition of 300 ppm NO exhibited almost the same effect on Hg⁰ removal. With further increasing the concentration of NO, the Hg⁰ removal efficiency increased gradually. The Hg⁰ removal efficiency was promoted to approximate 74.64 % with respect to 800 ppm NO,

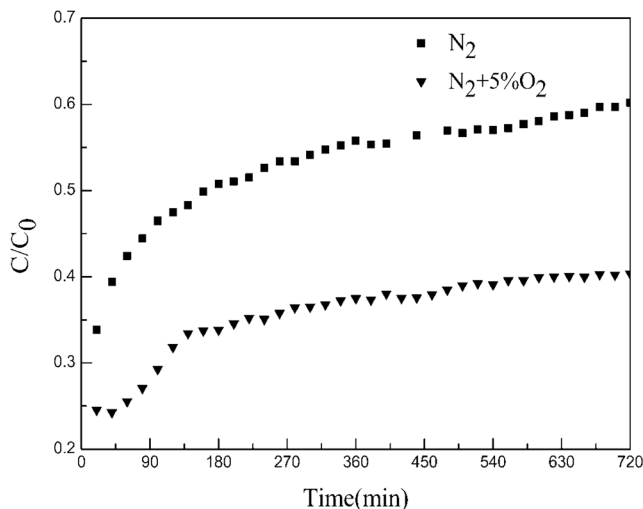


Fig. 9 Breakthrough curves of elemental mercury captured by Fe3Ce3/AC under N₂ and N₂ plus 5 % O₂. Reaction conditions: GHSV= 4200 h⁻¹, T=110 °C

which was even higher than that 5 % O₂ balanced with N₂ stream. The presence of Ce³⁺ on the sample surface was reported to promote the oxidation of NO-NO₂, and NO₂ was demonstrated to significantly improve heterogeneous oxidation of Hg⁰ over fly ash and activated carbon-based sorbents (Miller et al. 2000; Norton et al. 2003). Additionally, adding 5 % O₂ into 300 ppm, NO increased the Hg⁰ removal efficiency to about 90.63 %. What interests us is that the addition of 5 % O₂ coupled with 800 ppm NO into gas stream unexpectedly resulted in a distinct decrease of Hg⁰ removal efficiency. This phenomenon was in accordance with other researchers who hypothesized that HgO(ad) and NO might be generated between Hg⁰ and NO₂ (Norton et al. 2003). The excess addition of NO tends to drive the equilibrium to the left which will inhibit Hg⁰ oxidation by this mechanism:



Effect of SO₂

In literatures, the effect of SO₂ on Hg⁰ removal in the flue gas is complicated and not conclusive. Promotional (Eswaran and Stenger 2005; Li et al. 2011a), inhibitive (Ji et al. 2008; Li et al. 2010), and negligible effects (Li et al. 2008) have been reported. As shown in Fig. 8, when the concentration of SO₂ increased from 400 to 800 ppm, the Hg⁰ removal efficiency slightly decreased from 52.57 to 48.10 %. The addition of 1200 ppm SO₂ could achieve an insignificant promotional effect on Hg⁰ removal, and the removal efficiency increased to around 69.00 % by further increasing the concentration to 2000 ppm. Adding 5 % O₂ and 2000 ppm SO₂ into the gas stream, the Hg⁰ removal was greatly enhanced as shown in Fig. 8. This result indicated that SO₂ had a promotional effect on Hg⁰ removal with the aid of O₂. In the presence of gaseous O₂, abundant chemisorbed oxygen was generated due to Ce³⁺ related charge imbalance. SO₂ was oxidized to SO₃ by chemisorbed oxygen, which would generate new sites for Hg⁰ (Li et al. 2011b). Furthermore, SO₃ could react with Hg⁰ to produce HgSO₄ (Fan et al. 2010). The reactions are proposed as follows:



Effect of H₂O(g)

H₂O(g) is one of the main components in coal-fired flue gas and has inhibitive impacts on the activity of samples, so water resistance is an important parameter to assess for possible industrial application. H₂O(g) has been reported to inhibit Hg⁰ oxidation over metal oxide catalysts due to competitive

adsorption (Li et al. 2011a; Li et al. 2008). The same phenomenon was observed in our study. As listed in Fig. 8, the addition of 8 % H₂O(g) into SFG caused 15.29 % declination of Hg⁰ removal efficiency. The inhibitory effect of H₂O possibly came from its competitive occupancy of the available active sites and thus inhibited the Hg⁰ adsorption.

Conclusions

In the study, Fe₂O₃ and CeO₂ modified AC was prepared and applied to remove Hg⁰ from simulated flue gas in a lab-scale fixed-bed system at 50–200 °C. Results showed that impregnated AC samples had higher capacity for Hg⁰ removal compared to virgin AC. Particularly, when the mass ratio of Fe₂O₃ and CeO₂ was 3:3 and total mass percentage of Fe-Ce mixed oxides was 6 %, the Hg⁰ removal efficiency reached to an average of 88.29 % at 110 °C. Besides, the Hg⁰ removal efficiency was affected by flue gas components, therein, O₂ and NO were beneficial for Hg⁰ removal. SO₂ showed an insignificant inhibition for Hg⁰ removal, while it was observed to promote Hg⁰ removal in the presence of O₂. In addition, the Hg⁰ removal efficiency had a slight declination when H₂O (g) was added into the flue gas. The analysis of XPS indicated that the main species of mercury on used Fe₃Ce₃/AC was HgO, and the Hg⁰ oxidation benefited from lattice oxygen, chemisorbed oxygen, and/or weakly bonded oxygen species on the surface of Fe₃Ce₃/AC. Considering the necessity and cost savings, the following work should optimize the sample composition to investigate NO_x and Hg⁰ removal simultaneously.

Acknowledgments The project is supported by the National Natural Science Foundation of China (51278177, 51478173) and the National High Technology Research and Development Program of China (863 Program, No. 2011AA060803).

References

- Ayastuy J, Gil-Rodríguez A, González-Marcos M, Gutiérrez-Ortiz M (2006) Effect of process variables on Pt/CeO₂ catalyst behaviour for the PROX reaction. *Int J Hydrogen Energ* 31:2231–2242. doi:10.1016/j.ijhydene.2006.04.008
- Cao Y, Chen B, Wu J et al (2007) Study of mercury oxidation by a selective catalytic reduction catalyst in a pilot-scale slipstream reactor at a utility boiler burning bituminous coal. *Energ Fuel* 21:145–156. doi:10.1021/ef0602426
- Delgado J, Pérez-Omil J, Rodríguez-Izquierdo J, Cauqui M (2006) The role of the carbonaceous deposits in the catalytic wet oxidation (CWO) of phenol. *Catal Commun* 7:639–643. doi:10.1016/j.catcom.2006.02.003
- Deng S, Liu H, Zhou W, Huang J, Yu G (2011) Mn–Ce oxide as a high-capacity adsorbent for fluoride removal from water. *J Hazard Mater* 186:360–366

- Descostes M, Mercier F, Thromat N, Beaucaire C, Gautier-Soyer M (2000) Use of XPS in the determination of chemical environment and oxidation state of iron and sulfur samples: constitution of a data basis in binding energies for Fe and S reference compounds and applications to the evidence of surface species of an oxidized pyrite in a carbonate medium. *Appl Surf Sci* 165:288–302. doi:10.1016/S0169-4332(00)00443-8
- Dunham GE, DeWall RA, Senior CL (2003) Fixed-bed studies of the interactions between mercury and coal combustion fly ash. *Fuel Process Technol* 82:197–213. doi:10.1016/S0378-3820(03)00070-5
- Eom Y, Jeon SH, Ngo TA, Kim J, Lee TG (2008) Heterogeneous mercury reaction on a selective catalytic reduction (SCR) catalyst. *Catal Lett* 121:219–225. doi:10.1007/s10562-007-9317-0
- Eswaran S, Stenger HG (2005) Understanding mercury conversion in selective catalytic reduction (SCR) catalysts. *Energy Fuel* 19:2328–2334. doi:10.1021/ef050087f
- Fan X, Li C, Zeng G et al (2010) Removal of gas-phase elemental mercury by activated carbon fiber impregnated with CeO₂. *Energy Fuel* 24:4250–4254. doi:10.1021/ef100377f
- Fan X, Li C, Zeng G et al (2012) Hg⁰ removal from simulated flue gas over CeO₂/HZSM-5. *Energy Fuel* 26:2082–2089. doi:10.1021/ef201739p
- Galbreath KC, Zygarlicke CJ (2000) Mercury transformations in coal combustion flue gas. *Fuel Process Technol* 65:289–10. doi:10.1016/S0378-3820(99)00102-2
- Gao X, Jiang Y, Zhong Y, Luo Z, Cen K (2010) The activity and characterization of CeO₂-TiO₂ catalysts prepared by the sol-gel method for selective catalytic reduction of NO with NH₃. *J Hazard Mater* 74:34–39. doi:10.1016/j.jhazmat.2009.09.112
- Gillot B, Laarj M, Kacim S (1997) Reactivity towards oxygen and cation distribution of manganese iron spinel Mn_{3-x}Fe_xO₄ (0≤x≤3) fine powders studied by thermogravimetry and IR spectroscopy. *J Mater Chem* 7:827–831. doi:10.1039/A607179A
- Graat PC, Somers MA (1996) Simultaneous determination of composition and thickness of thin iron-oxide films from XPS Fe 2p spectra. *Appl Surf Sci* 100:36–40. doi:10.1016/0169-4332(96)00252-8
- He C, Shen B, Chen J, Cai J (2014) Adsorption and oxidation of elemental mercury over Ce-MnO_x/Ti-PILCs. *Environ Sci Technol* 48:7891–7898. doi:10.1021/es5007719
- Hsi HC, Lee HH, Hwang JF, Chen W (2010) Mercury speciation and distribution in a 660-megawatt utility boiler in Taiwan firing bituminous coals. *J Air Waste Manage Assoc* 60:514–522. doi:10.3155/1047-3289.60.5.514
- Hua X, Zhou J, Li Q, Luo Z, Cen K (2010) Gas-phase elemental mercury removal by CeO₂ impregnated activated coke. *Energy Fuel* 24:5426–5431. doi:10.1021/ef100554t
- Huang G, Liaw BJ, Jhang CJ, Chen YZ (2009) Steam reforming of methanol over CuO/ZnO/CeO₂/ZrO₂/Al₂O₃ catalysts. *Appl Catal A: Gen* 358:7–12
- Huang JY, Shao YX, Huang HG et al (2005) Binding mechanisms of methacrylic acid and methyl methacrylate on Si (111)-7×7 effect of substitution groups. *J Phys Chem B* 109:19831–19838. doi:10.1021/jp0531659
- Itaya Y, Kawahara K, Lee CW (2009) Dry gas cleaning process by adsorption of H₂S into activated cokes in gasification of carbon resources. *Fuel* 88:1665–1672. doi:10.1016/j.fuel.2009.04.005
- Jastrzab K (2012) Properties of activated cokes used for flue gas treatment in industrial waste incineration plants. *Fuel Process Technol* 101:16–22. doi:10.1016/j.fuproc.2011.05.028
- Ji L, Srekanth PM, Smirniotis PG, Thiel SW, Pinto NG (2008) Manganese oxide/titania materials for removal of NO_x and elemental mercury from flue gas. *Energy Fuel* 22:2299–2306. doi:10.1021/ef700533q
- Kamata H, Ueno SI, Sato N, Naito T (2009) Mercury oxidation by hydrochloric acid over TiO₂ supported metal oxide catalysts in coal combustion flue gas. *Fuel Process Technol* 90:947–951. doi:10.1016/j.fuproc.2009.04.010
- Kang M, Park ED, Kim JM, Yie JE (2007) Manganese oxide catalysts for NO_x reduction with NH₃ at low temperatures. *Appl Catal A: Gen* 327:61–269. doi:10.1016/j.apcata.2007.05.024
- Kaspar J, Fornasiero P, Graziani M (1999) Use of CeO₂-based oxides in the three-way catalysis. *Catal Today* 50:285–298. doi:10.1016/S0920-5861(98)00510-0
- Li H, Li Y, Wu CY, Zhang J (2011a) Oxidation and capture of elemental mercury over SiO₂-TiO₂-V₂O₅ catalysts in simulated low-rank coal combustion flue gas. *Chem Eng J* 69:86–93. doi:10.1016/j.cej.2011.03.003
- Li HL, Wu CY, Li Y, Zhang JY (2011b) CeO₂-TiO₂ catalysts for catalytic oxidation of elemental mercury in low-rank coal combustion flue gas. *Environ Sci Technol* 45:7394–7400. doi:10.1021/es2007808
- Li J, Yan N, Qu Z et al (2010) Catalytic oxidation of elemental mercury over the modified catalyst Mn/α-Al₂O₃ at lower temperatures. *Environ Sci Technol* 44:426–431. doi:10.1021/es9021206
- Li Y, Lee C, Gullett B (2003) Importance of activated carbon's oxygen surface functional groups on elemental mercury adsorption. *Fuel* 82:451–457. doi:10.1016/S0016-2361(02)00307-1
- Li Y, Murphy PD, Wu CY, Powers KW, Bonzongo JCJ (2008) Development of silica/vanadia/titania catalysts for removal of elemental mercury from coal-combustion flue gas. *Environ Sci Technol* 42:5304–5309. doi:10.1021/es8000272
- Li Z, Wu L, Liu H, Lan H, Qu J (2013) Improvement of aqueous mercury adsorption on activated coke by thiol-functionalization. *Chem Eng J* 228:925–934. doi:10.1016/j.cej.2013.05.063
- Liu TY, Liao HC, Lin CC, Hu SH, Chen SY (2006) Biofunctional ZnO nanorod arrays grown on flexible substrates. *Langmuir* 22:5804–5809. doi:10.1021/la052363o
- Milford JB, Pieniaci A (2009) After the clean air mercury rule: prospects for reducing mercury emissions from coal-fired power plants. *Environ Sci Technol* 43:2669–2673. doi:10.1021/es802649u
- Miller SJ, Dunham GE, Olson ES, Brown TD (2000) Flue gas effects on a carbon-based mercury sorbent. *Fuel Process Technol* 65:343–363. doi:10.1016/S0378-3820(99)00103-4
- Mullins D, Overbury S, Huntley D (1998) Electron spectroscopy of single crystal and polycrystalline cerium oxide surfaces. *Surf Sci* 409:307–319. doi:10.1016/S0039-6028(98)00257-X
- Norton GA, Yang H, Brown RC, Laudal DL, Dunham GE, Erjavec J (2003) Heterogeneous oxidation of mercury in simulated post combustion conditions. *Fuel* 82:107–116. doi:10.1016/S0016-2361(02)00254-5
- Ogriseck S, Vanegas GPG (2010) Experimental investigations of ammonia adsorption and nitric oxide reduction on activated coke. *Chem Eng J* 160:641–650. doi:10.1016/j.cej.2010.04.004
- Pavlish JH, Sondreal EA, Mann MD (2003) Status review of mercury control options for coal-fired power plants. *Fuel Process Technol* 82:89–165. doi:10.1016/S0378-3820(03)00059-6
- Pitoniak E, Wu CY, Mazyck DW, Powers KW, Sigmund W (2005) Adsorption enhancement mechanisms of silica-titania nanocomposites for elemental mercury vapor removal. *Environ Sci Technol* 39:1269–1274. doi:10.1021/es049202b
- Presto AA, Granite EJ (2006) Survey of catalysts for oxidation of mercury in flue gas. *Environ Sci Technol* 40:5601–5609. doi:10.1021/es060504i
- Reddy BM, Khan A, Yamada Y, Kobayashi T, Loridant S, Volta JC (2003) Structural characterization of CeO₂-TiO₂ and V₂O₅/CeO₂-TiO₂ catalysts by Raman and XPS techniques. *J Phys Chem B* 107:5162–5167. doi:10.1021/jp0344601
- Sahoo S, Mohapatra M, Pandey B, Verma H, Das R, Anand S (2009) Preparation and characterization of α-Fe₂O₃-CeO₂ composite. *Mater Charact* 60:25–431. doi:10.1016/j.matchar.2008.11.006
- Sakanishi K, Wu Z, Matsumura A (2005) Simultaneous removal of H₂S and COS using activated carbons and their supported catalysts. *Catal Today* 104:94–100. doi:10.1016/j.cattod.2005.03.060
- Shawwa AR, Smith DW, Segó DC (2001) Color and chlorinated organics removal from pulp mills wastewater using activated petroleum coke. *Water Res* 35:745–749. doi:10.1016/S0043-1354(00)00322-5

- Shen B, Liu T, Zhao N, Yang X, Deng L (2010) Iron-doped Mn-Ce/TiO₂ catalyst for low temperature selective catalytic reduction of NO with NH₃. *J Environ Sci* 22:1447–1454. doi:10.1016/S1001-0742(09)60274-6
- Wan H, Li D, Dai Y (2009) Effect of CO pretreatment on the performance of CuO/CeO₂/γ-Al₂O₃ catalysts in CO+O₂ reactions. *Appl Catal A: Gen* 60:26–2. doi:10.1016/j.apcata.2009.02.046
- Wan Q, Duan L, He K, Li J (2011) Removal of gaseous elemental mercury over a CeO₂-WO₃/TiO₂ nanocomposite in simulated coal-fired flue gas. *Chem Eng J* 170:512–517. doi:10.1016/j.cej.2010.11.060
- Wang X, Zheng Y, Lin J (2013) Highly dispersed Mn–Ce mixed oxides supported on carbon nanotubes for low-temperature NO reduction with NH₃. *Catal Commun* 7:96–99. doi:10.1016/j.catcom.2013.03.035
- Wen X, Li C, Fan X et al (2011) Experimental study of gaseous elemental mercury removal with CeO₂/γ-Al₂O₃. *Energ Fuel* 25:2939–2944. doi:10.1021/ef200144j
- Xie Y, Li C, Zhao L (2015) Experimental study on Hg⁰ removal from flue gas over columnar MnO_x-CeO₂/activated coke. *Appl Surf Sci* 333: 59–67. doi:10.1016/j.apsusc.2015.01.234
- Xu Z, Zhao L, Pang F, Wang L, Niu C (2007) Partial oxidation of methane to synthesis gas over hexaaluminates LaMA₁₁O_{19.5} catalysts. *J Nat Gas Chem* 6:0–63. doi:10.1016/S1003-9953(07)60027-9
- Yan N, Chen W, Chen J et al (2011) Significance of RuO₂ modified SCR catalyst for elemental mercury oxidation in coal-fired flue gas. *Environ Sci Technol* 45:5725–5730. doi:10.1021/es200223x
- Yang S, Zhu W, Jiang Z, Chen Z, Wang J (2006) The surface properties and the activities in catalytic wet air oxidation over CeO₂-TiO₂ catalysts. *Appl Surf Sci* 25:8499–8505. doi:10.1016/j.apsusc.2005.11.067
- Yue L, Zhang XM (2009) Structural characterization and photocatalytic behaviors of doped CeO₂ nanoparticles. *J Alloy Compd* 475:702–705. doi:10.1016/j.jallcom.2008.07.096
- Zhang A, Zheng W, Song J, Hu S, Liu Z, Xiang J (2014) Cobalt manganese oxides modified titania catalysts for oxidation of elemental mercury at low flue gas temperature. *Chem Eng J* 236:29–38. doi:10.1016/j.cej.2013.09.060